

Design and Instrumentation of Force Feedback in Telerobotics

Mayez A. Al-Mouhamed¹, Mohammad Nazeeruddin², and Nesar Merah³

Abstract—The design and instrumentation of force feedback (FF) is presented for a networked telerobotic system that consists of a Master Arm Client Station (MACS) and a Slave Arm Server Station (SASS). A motion coordination system maps the operator hand at MACS, to a user defined floating tool frame at SASS. Variational analysis for a wrist force sensor allows evaluating the force at a floating point of the tool frame. Force is streamed from SASS to MACS where it is displayed on the operator hand. Performance evaluation of contact with the environment is presented. First, a user-controlled teleoperation with FF is described. Contact instabilities are observed in pre-contact and post-contact phases. Second, a programmed compliance loop is implemented at SASS by selectively converting sensed forces into corrective motion which allows minimizing contact forces. Third, a supervisory mechanism based on a user-controlled *Active Compliance* is presented. High FF gain improves operator sensitivity but may cause instability in the case of contact with stiff environment. Motion mapping minimizes the number of trials to set up the tool configuration. Light and stiff arms are highly recommended to reduce the degradation in telerobotic synchronization caused by elasticity in linkage transmission and by the network delays. Active compliance at the slave arm improved contact stability and provided an effective supervisory control.

Index Terms—Distributed application framework, reflected force feedback, man-machine interface, Telerobotics.

I. INTRODUCTION

The usefulness of the force feedback in telerobotics has been demonstrated under simulated and real-world telerobotic systems. Modeling and simulating force sensors [1] enhances the accuracy of simulated dynamic interaction in virtual environment. For this a dynamic model of a six dofs force sensor with eight deformation components allows simulating the dynamic interaction between the sensor and the environment.

A six-axis force reflective hand controller (FRHC) [2] is evaluated using kinesthetic force feedback and stereo video. Evaluation of a drill task indicates equal task times but with noticeably lower cumulative variance and peak forces where either visual or kinesthetic force is used with stereo vision. Current-based force measurements at the slave arm can also be used as a measure of force [3] that can be feedback to the operator. A wearable low-cost control rig is designed to provide an intuitive force display. In addition, the operator feels the gripping force. The master and slave units interact

through an RF wireless mechanism. Haptic sensing is used to manipulate objects in the real world and to measure the rotational forces of the teleoperator.

To improve the accuracy of range measurements, a multimodal sensor system [4] is used to enhance the haptic control of robotic manipulations of small three-dimensional (3-D) objects. A 16×16 array of force sensing resistor elements are used to refine 3-D shape measurements which are monitored with a laser range finder. Small-size objects that cannot be accurately differentiated through range measurements are recognized with their orientation. A miniature force sensor [5] is proposed to measure the contact forces at the tip of a microsurgical instrument. A position-controlled motion is proposed with micrometer resolution for force-feedback of no less than 5 mN. The use of force-feedback in remote endoscopic surgery [6] proved to be beneficial. The slave manipulator accurately and quickly mimic the movement of the master arm at low speed; and the master arm satisfactorily reproduced the force.

Analysis of force feedback in micro-level tasks [7] allowed the design of a micro-gripper in which strain-gauge force sensors were interfaced to a haptic arm to let the operator feel the grasping forces and pulses in the micro vessels. This system was employed successfully to differentiate tiny samples (100 pico-meter width) of human skin which were freshly excised from the areas around the fingernails of three volunteers. In robotized surgery, force-feedback was used for patient motion-canceling [8] by minimizing forces due to accidental contact using the modulated impedance of the human hand. A task-oriented micro/nano space teleoperation system [9] used a mixture of direct and task oriented modes that were activated using a set of visualization and manipulation tools with some force monitoring. The high-level motion commands were used to avoid collisions. The approach was faster and safer with higher accuracy than the direct teleoperation given the presence of dominant electrostatic forces and the possibility of tool jams.

The system architecture of a real-time telerobotic client-server system is presented as a *Multithreaded Distributed Telerobotic Framework* [10] (MDTF). MDTF interacts through the Internet by using MSF .Net remoting technology. MDTF implements streaming of (1) operator commands, (2) video data, and (3) force feedback using robot kinematics and network programming tools. In this paper, we use MDTF as a testbed to study the mapping of motion coordination and force feedback. For this a wrist force sensor instrumentation model is presented. The model maps the forces exerted at a floating tool frame (slave arm) to operator hand (master arm).

(1) Department of Computer Engineering, College of Computer Science and Engineering (CCSE) King Fahd University of Petroleum and Minerals (KFUPM), Dhahran 31261, Saudi Arabia. mayez@ccse.kfupm.edu.sa

(2) Department of Systems Engineering, CCSE, KFUPM, Dhahran 31261, Saudi Arabia. nazeer@ccse.kfupm.edu.sa

(3) Department of Mechanical Engineering, KFUPM, Dhahran 31261, Saudi Arabia. nesar@kfupm.edu.sa

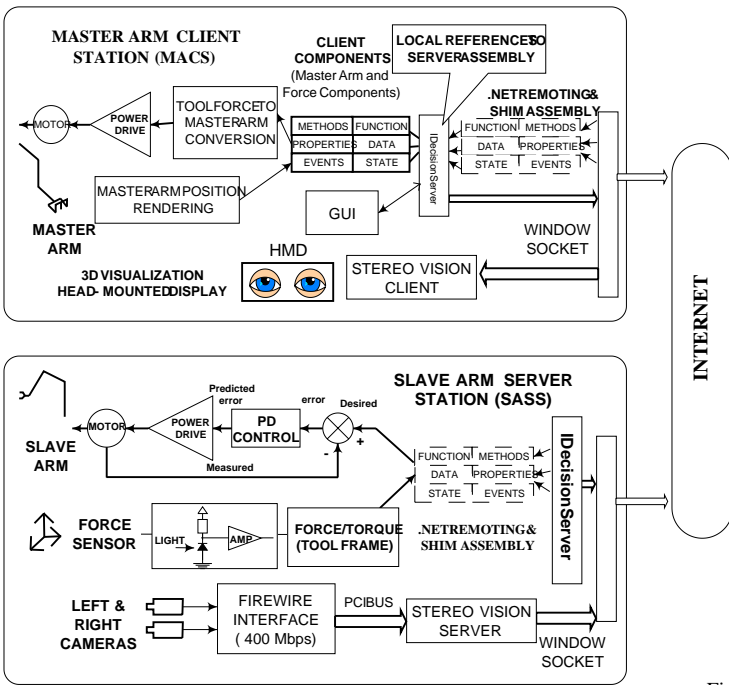


Fig. 1. Internet telerobotic system: real-time transfer of motion commands, force data, and stereo video from Server (SASS) to Client (MACS).

Instrumentation and measurement of real world teleoperation of contact between slave arm tool and environment is presented using (1) direct teleoperation with force feedback, (2) compliance mechanism at the slave arm, and (3) active compliance as a supervisory mechanism for networked teleoperation. Performance of contact tasks under each of the above schemes is investigated.

The paper consists of five sections. Section 2 presents an overview of a client-server networked telerobotic system. The wrist force sensor and its instrumentation model are described in section 3. The instrumentation analysis of teleoperation schemes is presented in section 4. Finally, section 5 presents a summary of the work along with the concluding remarks.

II. TELEROBOTIC SYSTEM

Telerobotics allows extending eye-hand motion coordination through a computer network. Motion scalability establishes a mapping from human scale to an arbitrary target scale (micro, nano, etc). Telerobotic performance is measured by: (i) the extent to which telerobotics preserves human manipulative dexterity and (ii) the fidelity in translating the physical laws from one scale to another. The most common architecture of a telerobotic system is based on a *Master Arm Client Station* (MACS) and *Slave Arm Server Station* (SASS) which are interconnected by a computer network integrating bilateral motion, cartesian motion coordination systems, teleoperation tools, stereo vision, and force feedback.

A schematic of the telerobotic system is shown in Figure 1. The SASS has three modules: (i) a PUMA slave arm module (S_{puma}); (ii) a force sensor module (S_{force}); and (iii) a video module (S_{video}). Similarly, the MACS also has also three modules: (i) a locally developed master arm operated by a client (C_{master}); (ii) a force display ($C_{force-disp}$);



Fig. 2. Master arm station: a user wearing a Head-Mounted Display (stereo vision) and tele-operating using a 6 dof anthropomorphic master arm for motion rendering and force display

and (iii) a video display ($C_{video-disp}$). The operator uses a light, 6 DOF, wire-based, anthropomorphic, master arm that was designed and manufactured at KFUPM. The telerobotic system software is implemented in a way that all the SASS and MACS modules run simultaneously as concurrent, independent, threads. The MACS client modules C_{master} , $C_{force-disp}$, and $C_{video-disp}$ are logically connected to the SASS server modules S_{puma} , S_{force} , and S_{video} , respectively. These modules interact through the network and forward their queries and available data in the real-time to the other modules.

The following is a short description of each module:

- 1) C_{master} regularly samples the master arm, computes variations in operator hand position using forward arm kinematics, and transfers position variation to S_{puma} .
- 2) S_{puma} receives variations in operator position, modifies slave arm tool position using inverse arm kinematics, and commands the slave motion accordingly.
- 3) S_{force} regularly samples wrist force sensors, evaluates the force applied to the tool, and streams the computed force to $C_{force-disp}$.
- 4) $C_{force-disp}$ receives force data, applies it to the master arm tool using the master arm variational model, and displays the force.
- 5) S_{video} continuously grabs video images from the left and right video cameras and transfers them to $C_{video-disp}$.
- 6) $C_{video-disp}$ displays the received stereo images using a Head-Mounted Display (HMD).

The MACS and SASS are implemented in client-server architecture that reliably transfers stereo, force, and command data. Moreover, MACS and SASS use the distributed software approach so that modification of a module in one station does not require any changes in the other station, i.e. the module functions are distributed in different software components. Specifically each module communicates with its counterpart

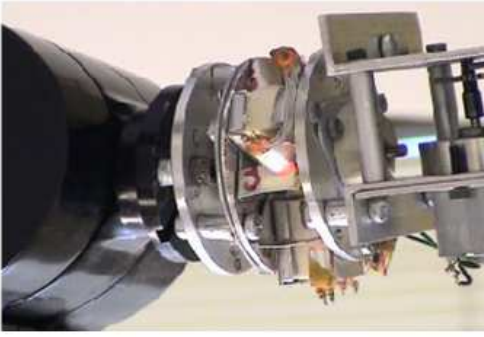


Fig. 3. Force sensor installed between the PUMA 560 wrist (left) and the gripper (right).

using a standard inter-process communication system. Here .NET remoting is used to publish the functions of the slave arm station (server) to any Internet connected master arm client [10]. The next section presents a wrist force sensor and its variational transformation model.

III. WRIST FORCE SENSOR

A wrist force sensor is used to provide both mechanical and electrical compliance at the tip of the slave robot arm. The electrical compliance or active compliance can be programmed to control the behavior of the slave arm in the presence of external forces. Its reaction depends on the activation of its control program. The presence of some passive mechanical compliance at the tip of the slave arm increases system reliability in assembly operations involving contact forces with unpredictable environment.

The force sensor (FS) is a wrist device that consists of two solid aluminum disks as shown in Figure 3. Each disk is 60 mm in diameter and 3 mm in thickness. The two disks are interconnected by means of three parallel cube-shaped rubber blocks which are mounted at (120°) to exhibit equal elasticity in all directions. FS is described in Figure 4-(a). Each sensor consists of an LED that generates a circular beam (3 mm diameter) of red light in front of a photo-transistor (PT). Each pair LED-PT is attached to the bottom disk. Two LED-PT sensors are placed at the left and right sides of each block. The sensors measure orthogonal displacements caused by an external force/torque applied on the top disk (tool), i.e. position and orientation displacement of tool with respect to arm wrist. For each sensor, a wing attached to upper disk is set to mask 50% of the light flowing from LED to PT. The PT output is proportional to the intensity of received light. It measures the directional displacement of tool with respect to arm wrist. For each block, the sensors are set to uncouple horizontal displacement from vertical displacement. Each wing measures displacement in one direction and is large enough to eliminate the effect of displacement in the two other directions as illustrated in Figures 4-(b) and (c). This allows uncoupling the vertical displacement from a possible horizontal displacement.

A. Sensor instrumentation model

The rubber blocks are attached to the disks at their contact bases. Since the wrist sensor is attached at the robot end, the

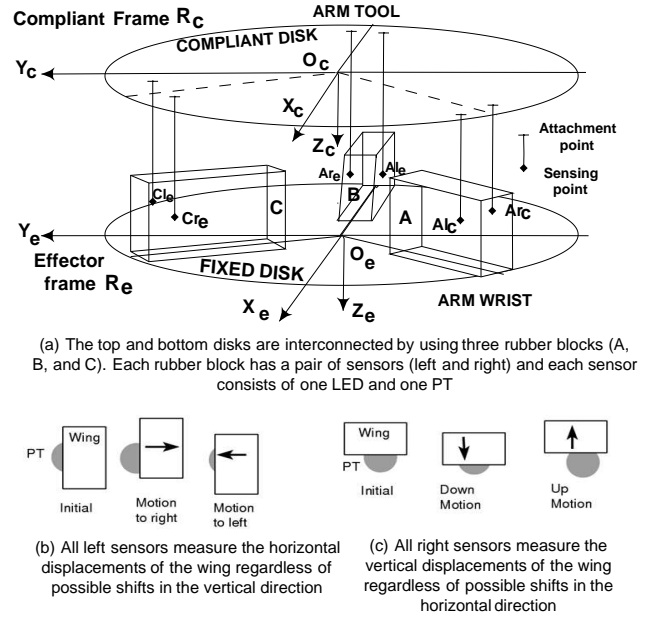


Fig. 4. Top and bottom sensor disks, frames, and sensing points (a), lateral motion sensing (b), and vertical motion sensing (c).

robot end frame R_e (effector) is located at the center of a fixed disk and a compliant frame R_c is placed at the center of the other disk. Any external force applied to the tool causes a deflection represented by a translation and rotation of R_c with respect to R_e .

The sensors are placed at the left and the right of each of the three rubber blocks denoted by A, B, and C. Each rubber block is surrounded by a left X_l and a right X_r sensing points, where X refers to rubber block A, B, or C. Since X_l is referenced in R_e , it is denoted by X_{le} . An external force and torque applied to tool, that is rigidly attached to R_c , causes: (1) translation of the origin of frame R_c by ΔX_e , and (2) a generalized rotation $M_{xyz}(\alpha, \beta, \gamma) = M_x M_y M_z$ of R_c with respect to R_e , where:

$$M_x(\alpha) = \begin{pmatrix} 1 & 0 & 0 \\ 0 & c\alpha & -s\alpha \\ 0 & s\alpha & c\alpha \end{pmatrix} \quad M_y(\beta) = \begin{pmatrix} c\beta & 0 & s\beta \\ 0 & 1 & 0 \\ -s\beta & 0 & c\beta \end{pmatrix}$$

$$M_z(\gamma) = \begin{pmatrix} c\gamma & -s\gamma & 0 \\ s\gamma & c\gamma & 0 \\ 0 & 0 & 1 \end{pmatrix} \quad (1)$$

The total differential of rotation matrix $M_{xyz}(\alpha, \beta, \gamma) = M_x M_y M_z$ is:

$$d(M_{xyz}(\alpha, \beta, \gamma)) = \frac{\partial M_x(\alpha)}{\partial \alpha} M_y M_z d\alpha + \frac{\partial M_y(\beta)}{\partial \beta} M_x M_z d\beta + \frac{\partial M_z(\gamma)}{\partial \gamma} M_x M_y d\gamma \quad (2)$$

It can be easily shown that for small angular variations α , β , and γ we have:

$$d(M_{xyz}(\alpha, \beta, \gamma)) = M_{\alpha, \beta, \gamma} = \begin{pmatrix} 0 & -\gamma & \beta \\ \gamma & 0 & -\alpha \\ -\beta & \alpha & 0 \end{pmatrix} \quad (3)$$

For a sensing point X_e that is observed in R_e , we have:

$$O_e X_e = O_e O_c + M_{xyz}(\alpha, \beta, \gamma) O_c X_c \quad (4)$$

where $O_e X_e$, $O_e O_c$, and $O_c X_c$ are the vectors of: (1) sensing point from the origin of R_e , (2) the origins of R_c from that of R_e , and (3) sensing point from the origin of R_c . Since an external force causes variation in the position ΔX_e and orientation $M_{\alpha, \beta, \gamma}$ of R_c , we have:

$$\Delta X_e = \Delta O_c + M_{\alpha, \beta, \gamma} O_c X_c \quad (5)$$

where ΔX_e and $\Delta O_c = (\Delta x, \Delta y, \Delta z)$ are the variations in the position at the sensing point and at the origin of R_c with respect to R_e , respectively. $O_c X_c$ is the fixed location of the sensing point observed in R_c . The problem is to compute translation ΔO_c of the compliance frame R_c and its elementary rotations α , β , and γ as function of sensor signal variations and location of sensing points. More specifically:

$$\Delta X_e = \begin{pmatrix} \Delta x \\ \Delta y \\ \Delta z \end{pmatrix} + \begin{pmatrix} 0 & -\gamma & \beta \\ \gamma & 0 & -\alpha \\ -\beta & \alpha & 0 \end{pmatrix} O_c X_c \quad (6)$$

Since each sensor can detect the motion of R_c in just one direction, only some components of ΔX_e are measurable. For example sensors located at Ar , Br and Cr detect translation of R_c plate only along the Z axis of R_e as illustrated on Figure 4-(a), i.e. the only measurable component of ΔAr_e is ΔAr_{ez} . If one rotates R_e about its Z axis by angles $u = \pi/6$ and $-u$, all the components of Bl , Al and Cl become directly measurable along the X and the Y axes of R_e , respectively.

Using Z components of equation 6, the sensors located at Ar , Br and Cr allow us to write:

$$\begin{pmatrix} \Delta Ar_{ez} \\ \Delta Br_{ez} \\ \Delta Cr_{ez} \end{pmatrix} = \begin{pmatrix} Ar_{cx} & Ar_{cy} & 1 \\ Br_{cx} & Br_{cy} & 1 \\ Cr_{cx} & Cr_{cy} & 1 \end{pmatrix} \begin{pmatrix} \beta \\ \alpha \\ \Delta O_{cz} \end{pmatrix} \quad (7)$$

The measurement $(\Delta Ar_{ez}, \Delta Br_{ez}, \Delta Cr_{ez})$ is used to compute $(\beta, \alpha, \Delta O_{cz})^t = M^{-1}(\Delta Ar_{ez}, \Delta Br_{ez}, \Delta Cr_{ez})^t$.

Using the X component of equation 6, the sensor located at Bl measures Bl_{ex} which is a force component along the X axis of R_e . This allows us to write:

$$\Delta Bl_{ex} = \Delta x - \gamma \times Bl_{cy} + \beta \times Bl_{cz} \quad (8)$$

All the components of Al and Cl are measurable along the Y axis of R_e , after rotating R_e about its Z axis by an angle u and $-u$, respectively. The implied change in the coordinate is represented by multiplying both sides of Equation 6 by the rotation matrix $M_z(u)$ given in Equation 1, i.e. $M_z(u)\Delta X_e$.

Using the Y component of $M_z(u)\Delta X_e$, the sensor located at Al (Cl) measures Al_{ey} (Cl_{ey}) which is a force component along the Y axis of R_e after affecting it by the above rotation matrices. Using rotation matrix $M_z(\pi/6)$ allows expressing the sensor data Al_{ey} as:

$$\Delta Al_{ey} = (c1 \times Al_{cx} + s1 \times Al_{cy})\gamma - (s1 \times \beta + c1 \times \alpha)Al_{cz} - s1 \times \Delta x + c1 \times \Delta y \quad (9)$$

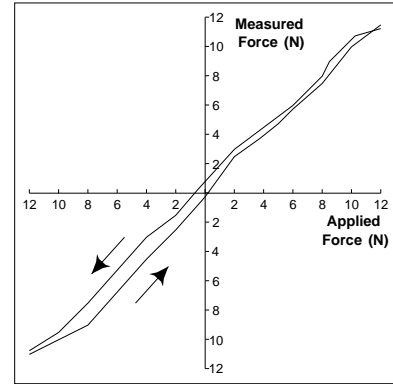


Fig. 5. Sensor characteristic: applied force (F_y) and computed force response based on measured wing displacements.

where $s1 = \sin(u)$ and $c1 = \cos(u)$. Similarly, the use of rotation matrix $M_z(-\pi/6)$ allows expressing the sensor data Cl_{ey} as:

$$\Delta Cl_{ey} = (c2 \times Cl_{cx} + s2 \times Cl_{cy})\gamma - (s2 \times \beta + c2 \times \alpha)Al_{cz} - s2 \times \Delta x + c2 \times \Delta y \quad (10)$$

where $s2 = \sin(-u)$ and $c1 = \cos(-u)$. Combining Equations 8, 9, and 10 we obtain:

$$\begin{pmatrix} \Delta Bl_{ex} - \beta \times Bl_{cz} \\ \Delta Al_{ey} + (s1 \times \beta + c1 \times \alpha)Al_{cz} \\ \Delta Cl_{ey} + (s2 \times \beta + c2 \times \alpha)Al_{cz} \end{pmatrix} = \begin{pmatrix} -Bl_{cy} & 1 & 0 \\ c1 \times Al_{cx} + s1 \times Al_{cy} & -s1 & c1 \\ c2 \times Cl_{cx} + s2 \times Cl_{cy} & -s2 & c2 \end{pmatrix} \begin{pmatrix} \gamma \\ \Delta x \\ \Delta y \end{pmatrix} \quad (11)$$

Denoting by U and M the vector and matrix that appear on the left hand side and right hand side of Equation 11, respectively results in $(\gamma, \Delta x, \Delta y) = M^{-1}U$, where ΔBl_{ex} , ΔAl_{ey} , and ΔCl_{ey} are the sensor data, and all the other variables are either known or already determined from Equation 6. All the variational parameters which are the translation $(\Delta x, \Delta y, \Delta z)$ and rotation (α, β, γ) are computable based on reading of the six sensor data and known sensor locations. Denote by $S_{stiffness}$ the sensor stiffness matrix of R_c with respect to R_e and let $\eta = (\Delta x, \Delta y, \Delta z, \alpha, \beta, \gamma)^t$. The generalized force/torque vector F measured by the sensor at O_e , the origin of R_e , is $F = S_{stiffness} \cdot \eta$.

F is the resultant of (1) the external force F_{ext} applied to the tool and measured at O_e , and (2) the generalized gravity vector $Q_e(\theta, \eta)$ measured at O_e , where θ is the arm joint vector. $Q_e(\theta, \eta)$ is caused by the gravity force applied at the center of mass of the body formed by the tool and gripper. Light loads cause small variations η of R_c with respect to R_e which allows writing $Q_e(\theta, \eta) \cong Q_e(\theta)$.

The measured force is then $F = S_{stiffness} \cdot \eta \cong F_{ext} + Q_e(\theta)$. Using FS to compute η , the external force applied to the tool is given by $F_{ext} \cong S_{stiffness} \cdot \eta - Q_e(\theta)$.

Computing F_{ext} may require on-line computation of $Q_e(\theta)$ [11] when a wide range of variations $\Delta \theta_{contact}$ is expected for the joint vector during the period of contact with the environment. Considering some useful θ configurations, a

lookup table can also be used to provide approximate values of $Q_e(\theta)$.

A heuristic approach can also be used when the variation $\frac{[Q_e]_{max} - [Q_e]_{min}}{[Q_e]_{min}}$ is expected to be small in the interval $\Delta\theta_{contact}$. One may compute the external force $F_{ext} \cong S_{stiffness} \cdot (\eta - \eta_{gravity})$, where $\eta_{gravity}$ is the gravity deflection of R_c with respect to R_e measured before contact with the environment.

The sensor was tested on the PUMA 560 robot arm, by applying selective forces/torque components at O_c , measuring the corresponding sensor wing displacements, and computing the variation vector η and the corresponding force $F = S_{stiffness} \cdot \eta$. F_y is plotted against the applied force $F_y(applied)$ on Figure 5. This figure can be considered as representative for the other force and torque features. The stiffness parameters for the diagonal components of $S_{stiffness}$ are estimated to: (1) (0.55, 0.67, 0.62) N/mm for force components, and (2) $(0.32, 0.47, 0.39) \times 10^{-1}$ Nm/mrd for torque components. The sensor measures linear force/torque up to ± 5 N with small wing displacements of ± 1.5 mm.

IV. INSTRUMENTATION ANALYSIS

Analysis of telerobotic delays through three campus routes was carried out by streaming of commands, force, and video. A sampling rate of 120 Hz is achieved for force feedback and 50 Hz for operator commands. Stereo video transfer operates at a rate of 17 frame per second. Total reference delays for force and video are 8 ms and 60 ms, respectively. Total round-trip delay (RTD) is 183 ms (5.5 Hz) when slave arm is operated at 10 Hz. Due to the mechanical delays of the PUMA slave arm and the stop-and-wait communication protocol between the client and server the sampling frequency of the local compliance loop was below 5 Hz. Bursty traffic load on the network causes variations (jitter) in control sampling. The system was tested using the following tasks: (1) peg-in-hole insertion, (2) assembly of a small water pump, (3) operating drawers, (4) pouring water, and (5) wire-wrapping. Video clips on these experiments can be found at [12].

A. Teleoperation with force feedback

In direct teleoperation the operator (1) uses a master arm to prescribe his hand motion to slave arm, and (2) feels the coordinated force feedback as displayed on the master arm motors to reproduce the slave tool force at the operator hand. The objective is to study the contact made between the slave arm tool and the environment. There are three phases in operation: (1) pre-contact, (2) contact, and (3) pre-release. The operator is provided with a force display. The operator moves the slave arm to cause a contact with some object. While feeling the contact force the operator is asked to exert and maintain a force of 1 N on the target for no less than 3 seconds prior to the release. A force feedback gain (FFG) is used to adjust the displayed force value to a proper sensitivity level for the operator. The master arm can display up to ± 15 N force in any direction.

Figure 6 shows the interaction during contact between the tool and (1) a rubber (Plots a and b), (2) a human muscle tissue (plots c and d), and (3) rigid body (plot e and f). For each of

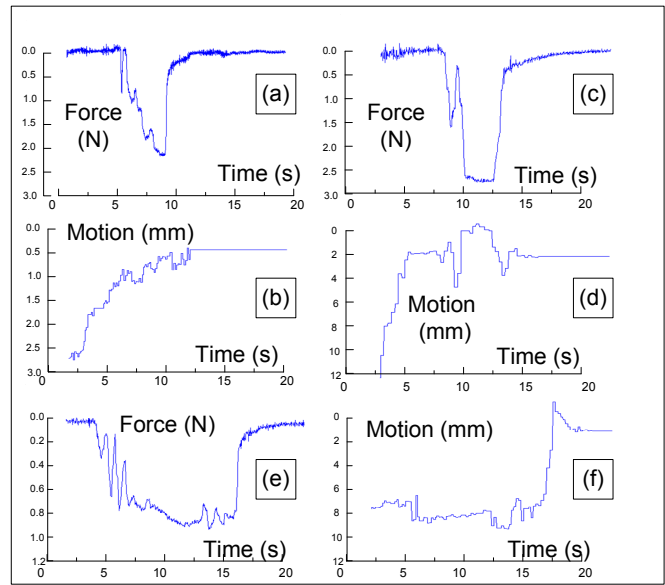


Fig. 6. Bilateral teleoperation with reflected force feedback ((a), (c), and (e) and corresponding user motion correction ((b), (d), and (f)

the above three cases the plot shows the force measured at the slave arm tool (plots a, c, and e) and motion reaction (plots b, d, and f) made by the operator at master arm to zero the displayed force feedback. Following the contact, the operator needs not return to the initial position because the object was lightly pushed by the exerted force.

In general, both the pre-contact and pre-release phases are subject to instability. For low values of FFG (below 5) the operator does not properly feel the contact. For moderate values of FFG (from 10 to 20) the force feeling is appropriate but with the instability shown in the pre-contact (also in pre-release). For higher values of FFG the teleoperation becomes dominated by instability which is driving the operator. The operator needs to adjust the displayed force gain to a proper sensitivity level in connection with overall system stability. In the contact phase the operator feels the wall effect as the master arm produces a repulsive force constraining the operator motion in the direction that increases the above constraints.

The instability and its vibration frequency depend on: (1) the stiffness of the target, (2) value of FFG, and (3) the system RTD of 183 ms excluding operator time. Stiff targets produce prompt bouncing forces with higher vibration frequencies (plots e-f)). The vibrations for rigid objects are greater and faster than those of the rubber or the tissue. Contact forces return a bouncing force from the operator. This process continues until the contact is firmly engaged which damps out the vibrations. A high feedback gain and a fast contact may drive the telerobot out of control, i.e. the master arm becomes instable which makes teleoperation quite poor. Stable contact for the rigid and rubber objects requires the use of moderate gains (less than 20) as compared to the case of the tissue.

B. Active compliance at the slave station

Implementing active compliance (AC) consists of activating a local control loop, at the slave arm station, in which the measured tool force at a selected compliance center is

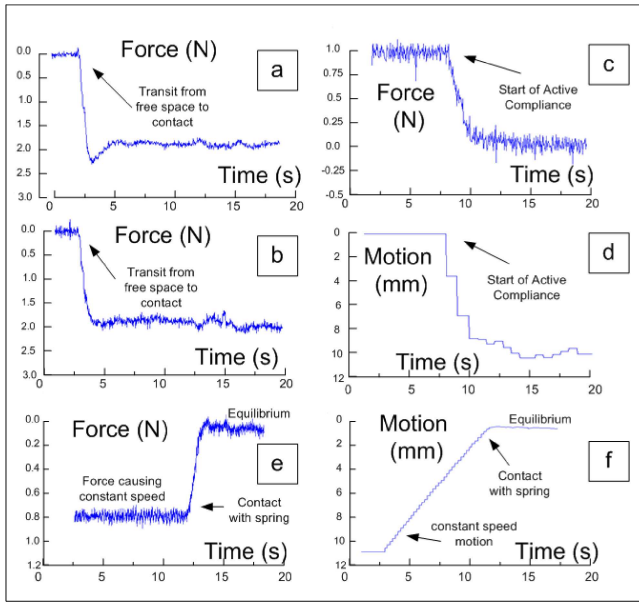


Fig. 7. Active compliance functions at the server station

converted into a corrective position or velocity. Due to stop-and-wait protocol between the master and slave systems the AC loop runs once for each arrival of a master arm command. The AC experiments are the following:

- 1) The tool frame is moved at constant speed in one horizontal direction while the vertical direction is under force control with a desired force of 2N. A peg ended with a rolling wheel is attached to the tool. The wheel hits an inclined plan (20°) and the force regulation lead the tool to climb up the plane. A desired downward force F_d is applied to maintain contact. AC consists of a applying motion correction defined by $\Delta T = A(F_d - F_t)$. F_d is applied following the first contact. F_d is selected and set through the client user interface. Figure 7-(a) shows the measured force during the motion where the dynamic force is very close to the desired value but with some overshoot. Figure 7-(b) shows the measured force when the motion correction contains a damping term defined as $\Delta T = A_p(F_d - F_t) - A_v \dot{F}_t$, where \dot{F}_t is the time derivative of measured force and A_p and A_v are two gain matrices.
- 2) The tool is manually moved to press a spring and instantly released. Figures 7-(c) and (d) shows the measured force as caused by the spring reaction and the position corrections made by the active compliance controller according to $\Delta T = A(F_{spring} - F_t)$, where F_{spring} is the spring force exerted on the tool. The corrections made by the active compliance controller iteratively reduce the resulting force (compliance) on the tool. At equilibrium the tool converges to a position where the external force is null.
- 3) A weight of 0.8N is set on the tool causing a vertical motion of the tool. A spring is placed in the motion direction. When the tool (with weight) hits the spring the measured force is nearly zero due to balancing between the gravity induced by the weight and the spring reaction

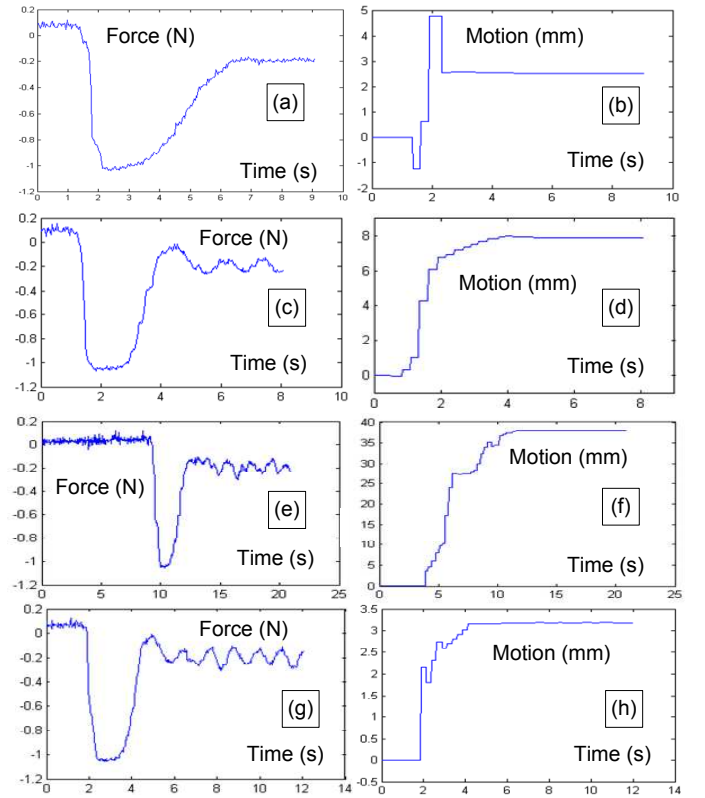


Fig. 8. Shared-control using active compliance and bilateral teleoperation with reflected force feedback ((a), (c), and (e) and corresponding AC's motion correction ((b), (d), and (f) to zero the force.

to the above force. Figures 7-(e) and (f) show that the transient force and the converging position.

C. Teleoperation using AC

Teleoperation with AC consists of direct teleoperation with display of force feedback and the active compliance AC is activated at the slave site to shorten the force interaction loop.

Figure 8 shows the generated force feedback and the implied position corrections carried out by AC. Figures 8-(a), (c), (e), and (g) show the force measured at the tool during contact with a spring, rubber, tissue, and a rigid object, respectively. The corrective motion carried out by the active compliance in each of the above cases are shown on Figures 8-(b), (d), (f), and (h), respectively. The stair shape in position corrections is caused by the stop-and-wait protocol (client and server) and jitter in the control inter-arrival times due to instantaneous variations in network traffic load.

The position corrections ΔT made by the active compliance controller are proportional to force error defined as $\Delta T = A_p(F_d - F_t)$, where A_p is a gain matrix. The corrections made by the active compliance controller are effective to reduce the contact forces. These corrections cause the contact force to return to zero level at different speed depending on the contacted object. Slow and smooth return to zero is found in the case of the spring. However, in all of the other three observed cases some oscillations are taking place at equilibrium, i.e. at convergence of corrections or pre-release phase. The largest oscillations are observed in the case of the rigid object.

The success of direct teleoperation with AC (shared control) is due to its locality which avoids communication delays and its adaptation to sensed forces which avoid a non-linear and late operator reaction.

V. CONCLUSION

A wrist force sensor is proposed to measure the force feedback for a master-slave telerobotic system. An instrumentation model of the sensor is proposed for computing the force/torque vector exerted at a floating tool frame based on measured elementary displacements in the sensor. Instrumentation analysis of contact between the slave arm tool and the environment has been carried out using three settings. In direct teleoperation, the force feedback generated out of user-controlled contact exhibited some instability due to linkage elasticities in pre- and post-contact phases. A qualitative contact characterization is presented based on force feedback gain and environment impedance. To reduce environment variations an active compliance mechanism is proposed as a local loop (fine corrections) at the slave arm to minimize contact forces. It acts by converting sensed forces into corrective motions to zero external forces. The operator carries out coarse teleoperation of the slave arm. This scheme resembles a two-level subsumptive control.

ACKNOWLEDGMENT

Thanks for King Abdulaziz City for Science and Technology (KACST) and KFUPM for computing support.

REFERENCES

- [1] Y.F. Li and J. Wang. Incorporating contact sensing in virtual environment for robotic applications. *IEEE T. on Instrumentation and Measurement*, 48(1):102 – 107, 1999.
- [2] L.E.P. Williams, R.B. Loftin, H.A. Aldridge, E.L. Leiss, and W.J. Bluethmann. Kinesthetic and visual force display for telerobotics. *IEEE Inter. Conf. on Robotics and Automation, ICRA '02*, 2:1249–1254, 2002.
- [3] G. S. Gupta, S. C. Mukhopadhyay, C. H. Messom, and S. N. Demidenko. Masterslave control of a teleoperated anthropomorphic robotic arm with gripping force sensing. *IEEE T. on Instrumentation and Measurement*, 55(6):2136 – 2145, 2006.
- [4] P. Payeur, C. Pasca, A.-M. Cretu, and E.M. Petriu. Intelligent haptic sensor system for robotic manipulation. *IEEE T. on Instrumentation and Measurement*, 54(4):1583 – 1592, 2005.
- [5] P.J. Berkelman, L.L. Whitcomb, R.H. Taylor, and P. Jensen. A miniature microsurgical instrument tip force sensor for enhanced force feedback during robot-assisted manipulation. *IEEE Trans. on Robotics and Automation*, 19:5:917–921, Oct. 2003.
- [6] A. Matsui, K. Mabuchi, T. Suzuki, A. Namiki, M. Ishikawa, H. Fujioka, and H. Ishigaki. Development of a remotely-operated master-slave manipulation system with a force-feedback function for use in endoscopic surgery. *IEEE Inter. Conf. on Eng. in Medicine and Biology*, 2:1260 – 1263, July 2000.
- [7] A. Menciassi, A. Eisinger, G. Scalari, C. Anticoli, M.C. Carrozza, and P. Dario. Force feedback-based microinstrument for measuring tissue properties and pulse in microsurgery. *IEEE Inter. Conf. on Robotics and Automation*, 1:626–631, 2001.
- [8] C.W. Kennedy and J.P. Desai. Enabling technologies for robotically-assisted sutureless coronary anastomosis. *Proc. 2005 IEEE Int. Conf. on Robotics and Automation*, pages 2927–2932, 2005.
- [9] A. Codourey, M. Rodriguez, and I. Pappas. A task-oriented teleoperation system for assembly in the microworld. *Proc. 8th International Conference on Advanced Robotics, 1997. ICAR '97*, pages 235–240, July 1997.
- [10] M. Al-Mouhamed, O. Toker, and A. Iqbal. A multi-threaded distributed telerobotic framework. *IEEE Trans. on Mechatronics*, 11(5):558–566, October 2006.
- [11] A. Izaguirre and R. Paul. Mcomputation of the inertial and gravitational coefficients of the dynamics equations for a robot manipulator with a load. *Proc. IEEE Inter. Conf. on Robotics and Automation*, 2:1024 – 1032, 1985.
- [12] Video clips. <http://www.ccse.kfupm.edu.sa/researchgroups/robotics3>.